ELSEVIER

Biophysical Chemistry 74 (1998) 209–224

Biophysical Chemistry

Magnetic field perturbations as a tool for controlling enzyme-regulated and oscillatory biochemical reactions

C. Eichwald, J. Walleczek*

Bioelectromagnetics Laboratory, Department of Radiation Oncology, School of Medicine-AO38, Stanford University, Stanford, CA 94305-5304, USA

Received 21 October 1997; received in revised form 23 June 1998; accepted 25 June 1998

Abstract

The feasibility of magnetic field perturbations as a tool for controlling enzyme-regulated and oscillatory biochemical reactions is studied. Our approach is based on recent experimental results that revealed magnetic field effects on the in vitro activity of enzyme systems in accordance with the radical pair mechanism. A minimum model consisting of two coupled enzyme-regulated reactions is discussed that combines, in a self-consistent manner, magnetic field-sensitive enzyme kinetics with non-linear dynamical principles. Furthermore, a simple detector mechanism is described that is capable of responding to an oscillatory input. Results reveal that moderate-strength magnetic fields ($B = 1–100$ mT) may effectively alter the dynamics of the system. In particular, a response behavior is observed that depends on: (1) the combination of static and time-varying magnetic fields; (2) the field amplitude; and (3) the field frequency in a non-linear fashion. The specific response behavior is critically determined by the biochemical boundary conditions as defined by the kinetic properties of the system. We propose an experimental implementation of the results based on the oscillatory peroxidase–oxidase reaction controlled by the enzyme horseradish peroxidase.

Keywords: Non-linear oscillators; Enzyme kinetics; Decoding mechanisms; Magnetic field effects; Radical pair mechanism

1. Introduction

Time-varying external perturbations are utilized in an increasing number of studies to investigate and control the dynamical behavior of excitable chemical, biochemical as well as biological systems [1–9]. Excitable systems are capable of displaying complex responses towards perturbations with time-varying external stimuli. Experimental examples include studies wherein either oscillatory concentrations of chemical species are applied, or feedback control techniques are utilized in the perturbation of the system. The latter technique has been demonstrated, for example, in

* Corresponding author. Tel.: +1 650 4985521; fax: +1 650 4985523; e-mail: jan.walleczek@forsythe.stanford.edu

0301-4622/98/$19.00
PII S0301-4622(98)00180-X

controlling chaos in the oscillatory Belousov–Zhabotinsky (BZ) reaction [1]. The same principles were also applied to biological systems, including the control of cardiac chaos [4] and brain chaos [5]. Recently, periodic perturbations of intracellular calcium or inositol 1,4,5-trisphosphate (IP_3) concentrations have been shown to control the activation of certain cancer cell genes in non-linear dependence on perturbation frequency [6,7]. Periodically varying modulations of the oxygen supply were utilized to study the response behavior of the peroxidase–oxidase oscillator [8]. The latter is controlled by the horseradish peroxidase enzyme [9].

In addition to chemical stimuli, there are other studies wherein physical stimuli including light and electric fields were successfully applied as initiators or modulators of dynamical behavior. For example, oscillating light stimuli were shown to induce coherent oscillations in the electric field gradient across a lipid membrane containing light-sensitive bacteriorhodopsin molecules [10]. The effect revealed a non-linear dependence on the frequency of the stimulation. In the light-sensitive BZ reaction dramatic changes in the formation of rotating spiral waves have been reported [2]. Again this effect was strongly dependent on the frequency of the light stimulus. In a similar fashion electric fields have been applied to perturb the dynamical behavior of spiral-shaped excitation patterns in the BZ reaction [11]. In a recent study optical forcing has been utilized to induce resonant standing-wave patterns in the BZ reaction [12].

Oscillating electric field stimuli were applied to investigate the dynamical behavior of electrically-excitable tissues. The chaos control studies mentioned above belong to this group of experiments. In other studies the stimulation of cardiac cells with a range of electric field frequencies, $\nu = 2–20$ Hz, was shown to induce sharp, frequency-dependent transitions between periodic and chaotic dynamical states in cell electrical activity [13]. Similarly, neuronal signal amplification was observed to depend in a non-linear fashion on the frequency of the imposed electrical stimulus ($\nu =$ 10–100 Hz) [14]. An optimum response resulted at an intermediate frequency. Alternating electric currents were applied in a recent study of the BZ and peroxidase–oxidase reactions [15].

The common basis enabling the occurrence of such a frequency-dependent response behavior to either chemical perturbations, light stimuli or electrical signals is that there exists a microscopic physicochemical process that (1) is sensitive towards the specific type of perturbation; and (2) is central to the generation or maintenance of the dynamics at the macroscopic level. Because of the apparent universality of the phenomena described above, the question arises whether there are other stimuli that may be utilized to perturb dynamical behavior within biologically relevant processes.

In recent years experimental results have revealed that magnetic fields of moderate field amplitudes ($B = 1–100$ mT) may alter the activity of certain enzyme reactions [16,17]. In particular, it was shown that the in vitro activity of coenzyme B_{12}-dependent ethanolamine ammonia lyase is magnetic field-sensitive [18,19]. Experimental investigations revealed that magnetic fields of approx. $B = 100$ mT magnetic flux density reduce the V_{max}/K_M kinetic parameter of the enzyme reaction by 25%. In a recent study it was reported that the redox cycling of horseradish peroxidase may be altered by magnetic fields [20]. This is the same enzyme that controls the dynamical peroxidase–oxidase system. An interpretation of the magnetic field-dependencies observed in the enzyme reactions is based on the radical pair mechanism [16,21]. This mechanism is a well-established tool for interpreting magnetic field influences on chemical as well as biochemical reactions that proceed via radical pair-dependent processes [22–25].

The discovery of magnetic field-sensitive processes in biological systems in combination with a well-established interaction mechanism raises an interesting possibility. Magnetic field stimuli could be applied as a minimally-invasive tool for perturbing biochemical or biological systems in a fashion analogous to the use of oscillating chemical, light or electrical stimuli. Hence, the motivation for the work described here is to discuss a minimum model that accounts in a consistent manner for magnetic field influences

on an oscillatory biochemical reaction. In the following section we describe general aspects of the model regarding potential biological implementations. Then the model and the calculations are outlined. In the subsequent section the behavior of the model system is studied under the influence of static as well as oscillating magnetic field perturbations. Finally, we introduce a simple detector mechanism that is capable of responding to magnetic field perturbations on the oscillatory dynamics of the biochemical reaction. We conclude by proposing a possible experimental implementation of the results.

2. Magnetic field perturbation of oscillatory biochemical reactions

2.1. Basic principles underlying the model

We study a prototypical model of two coupled enzyme-regulated reactions (Fig. 1). The system represents a cyclic reaction wherein substrate S is converted into product P catalyzed by enzyme reaction E_1, and subsequently product is converted back into substrate catalyzed by enzyme reaction E_2. The designations substrate and product are of course interchangeable, because of the cyclic nature of the system. It is implicitly assumed that one of the reactions includes an energy conversion step, for example, by hydrolysis of adenosine triphosphate (ATP), to drive the reaction against a concentration gradient [26]. Systems consisting of two connected elements such as the coupled enzyme-regulated reaction depicted in Fig. 1 are commonly encountered within biochemical reaction networks [27,28]. Independently of the specific details, the principle of a coupled reaction cycle is central to several enzyme-dependent biological activities. In particular, schemes including phosphorylation/dephosphorylation cycles catalyzed by a protein kinase and a protein phosphatase, respectively, have been discussed by several groups [29–34]. In this case the system consists of an interconvertible enzyme in an inactive and an active state, rather than substrate and product as in Fig. 1. At the cellular level, although vastly more complex in detail, one

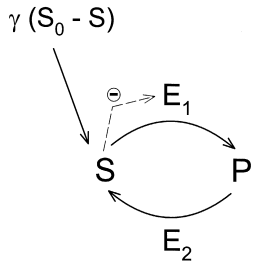

Fig. 1. Scheme of the model of two coupled enzyme-controlled reactions. Substrate S is being converted into product P catalyzed by enzyme reaction E_1. Subsequently, product is converted back into substrate catalyzed by enzyme reaction E_2. It is assumed that one of the reactions includes an energy conversion step. Substrate is supplied at a net rate of $\gamma(S_0 - S)$. The activity of enzyme E_1 is controlled by substrate inhibition kinetics, as indicated by the minus sign in the figure.

scheme demonstrating this principle is the cytosolic calcium oscillator. Cytosolic calcium cycling is controlled by the IP_3 receptor channel (IP_3R), leading to the release of calcium, and the calcium ATPases that transport calcium back into the stores [35,36]. In this case, substrate S in the scheme, Fig. 1, may be identified with cytosolic calcium, whereas product P represents the calcium content of an intracellular store. Finally, tank-reactor studies with the oscillatory peroxidase–oxidase reaction system provide another example. In these experiments a recycling system involving two enzymes is often utilized [3,8,37–42]. This system consists of horseradish peroxidase, which catalyzes the aerobic oxidation of NADH to NAD^+, and glucose-6-phosphate dehydrogenase. The latter catalyzes the conversion of NAD^+ back into NADH. Conceptually this experimental scheme closely resembles the one shown in Fig. 1.

In this modeling study of an elemental coupled-enzyme reaction the following specific case is investigated: (1) the activity of one of the enzymes is controlled by substrate inhibition kinetics; and (2) the activity of the other enzyme exhibits magnetic field sensitivity. The first condition enables the inclusion of regulatory feedback mechanisms. Under the appropriate boundary conditions this may lead to a system that is capable of sustained oscillatory behavior, since substrate inhibition kinetics offers one pathway for

inducing enzyme-regulated biochemical oscillations [43]. For example, negative feedback regulation by calcium on the opening probability of the IP_3R is regarded as a crucial process in the formation of cytosolic calcium oscillations [35,36,44]. In the case of the peroxidase–oxidase system, negative feedback regulation again is essential to the generation of sustained oscillations in enzyme activity [45].

The simple reaction scheme depicted in Fig. 1 enables studies of the influence of external magnetic fields, including constant and time-varying ones, on an oscillatory biochemical reaction. The structure of the model offers several advantages. In particular, the separation of regulatory feedback control and magnetic field-sensitivity into two enzyme-regulated reactions makes it possible to use an existing model for describing magnetic field effects on enzyme kinetics without the necessity for further modifications [21,46]. At the same time complex regulatory mechanisms may be introduced into the system via the magnetic field-independent enzyme reaction.

Independently of specific realizations, it has been discussed recently that cyclic reactions provide a basis for operating as computational elements within complex biochemical reaction networks [27,28]. In this approach cyclic reactions function as an integral part of the reaction network by conveying information between the individual elements. Therefore, at least in principle, the scheme depicted in Fig. 1 may also serve as a system for studying magnetic field influences on a non-linear biochemical reaction from the perspective of biological information processing.

The preceding discussion suggests that the model may serve as a general approach towards studying magnetic field influences on an oscillatory biochemical reaction. In particular, the nonlinear dynamical nature of the model makes it possible to investigate magnetic field influences that may depend on (1) the field frequency; (2) the field amplitude; (3) the combination of static and time-varying fields; and (4) the biological state of the system. The latter aspect is related to the biochemical boundary conditions as defined by the kinetic parameters of the enzyme-controlled reactions [47].

2.2. Outline of the model and calculations

The following mechanism including substrate inhibition is studied in regards to the enzyme reaction controlled by E_1:

$$E_1 + S \underset{k_{-11}}{\overset{k_{11}}{\rightleftharpoons}} (E_1S), (E_1S) \underset{k_{-12}}{\overset{k_{12}}{\rightleftharpoons}} E_1 + P, (E_1S) + S \underset{k_{-I}}{\overset{k_I}{\rightleftharpoons}} (SE_1S), \qquad (1)$$

where the forward (backward) rate constants are denoted as $k_i(k_{-i})$, and the other symbols represent: E_1, enzyme, S, substrate, (E_1S), enzyme–substrate complex with one substrate molecule bound, (SE_1S), enzyme–substrate complex with two substrate molecules bound (one at the active site and the other one at an inhibitory site). The mechanism described by Eq. (1) is a standard one. It has been applied, for example, in early studies to illustrate the possibility of bistability caused by substrate inhibition in the peroxidase system [45].

We assume that the second enzyme reaction controlled by E_2 exhibits magnetic field sensitivity. A model is applied that has been developed to interpret magnetic field effects on the reaction kinetics of enzymes that exhibit radical pair recombination steps in their reaction cycle [21,46]. The model combines chemical kinetics with magnetic field-dependent spin kinetics (radical pair mechanism). The reaction scheme reads as follows:

$$\begin{array}{l} E_2 + P \underset{k_{-21}}{\overset{k_{21}}{\rightleftharpoons}} (E_2P) \underset{k_{-22}}{\overset{k_{22}}{\rightleftharpoons}} {}^{S}(E_2^{\bullet\bullet}P) \searrow^{k_{32}} \\ \qquad\qquad\qquad\qquad \downarrow \uparrow k_{\mathrm{isc}} \\ \qquad\qquad\qquad\qquad {}^{T}(E_2^{\bullet\bullet}P) \nearrow_{k_{32}} \underset{E_2+S}{\downarrow k_{42}} \end{array} \qquad (2)$$

where the symbols represent: E_2, enzyme, (E_2P), enzyme–substrate complex prior to radical pair-generation, ${}^{S/T}(E_2^{\bullet\bullet}P)$, enzyme–substrate complex where a spin-correlated radical pair exists, $(E_2P)^*$, enzyme–substrate complex prior to

product release (note that the term substrate of E_2 is equivalent to the product of E_1). The superscript denotes spin multiplicity (S, singlet, T, triplet), and k_{isc} is a magnetic field-dependent rate constant characterizing singlet–triplet mixing. A short-hand notation, ${}^{T}(E_2^{\bullet\bullet}P)$, representing all three triplet states $T \rightarrow \{T_{-1}, T_0, T_{+1}\}$ is used (the index refers to the magnetic quantum number).

In the reaction scheme of Eq. (2), radical pair generation is via k_{22}, and recombination via k_{-22}. The rate constant k_{32} characterizes the spin-independent forward reaction coordinate motion. It is used here to represent the lifetime of the spin-correlated radical pair state. The magnetic field sensitivity arises solely from the modulation of the population of the singlet and triplet states via k_{isc} leading to a net change in the concentration of ${}^{S}(E_2^{\bullet\bullet}P)$ and of ${}^{T}(E_2^{\bullet\bullet}P)$. This modulation can directly affect the enzyme reaction cycle because — as a consequence of the Pauli principle — only ${}^{S}(E_2^{\bullet\bullet}P)$, but not ${}^{T}(E_2^{\bullet\bullet}P)$ can recombine via k_{-22} (radical pair recombination) to yield (E_2P); that is, a magnetic field-induced change in $[{}^{S}(E_2^{\bullet\bullet}P)/{}^{T}(E_2^{\bullet\bullet}P)]$ leads to a corresponding (spin-dependent) change in k_{-22} and thus k_{22} enabling a field effect on the enzyme reaction pathway. All subsequent processes preceding product release via k_{42} are not considered to exhibit a requirement for spin correlation. The enzyme reaction scheme exhibits transitions between different states that operate on very different time scales. This is a result of combining processes related to chemical kinetics and to magnetic field-dependent spin kinetics. The rate constants k_{-22} (radical pair recombination), k_{32} (forward reaction coordinate motion) and k_{isc} (singlet–triplet mixing) represent fast time-scales in the 1–100-ns time domain. Consequently the concentrations of the radical pair states, ${}^{S/T}(E_2^{\bullet\bullet}P)$, are small and rapidly converge to the steady-state value. The remaining rate constants are related to the much slower processes within the enzyme reaction cycle.

The introduction of an effective rate constant, k_{isc}, characterizing singlet–triplet mixing is based on the assumption of steady state kinetics for describing the radical pair system [46]. It is assumed that the temporal variations of the magnetic field are much slower than the radical pair lifetime, which typically is in the range of 1–100 ns [22,24,25]. Within this time frame the radical pair senses a quasi static magnetic field [48]. Therefore spin evolution of the radical pair may be regarded as a quasi steady state process on the time scale of the magnetic field variations. In this case the quantum-statistical equations describing spin evolution of the radical pair may be solved under static magnetic field conditions and the actual value of the magnetic flux density may be substituted to calculate the effect of the slowly-varying magnetic field.

Under the conditions outlined above it is possible to define an effective rate constant $k_{22,eff}$ that characterizes net forward flux between the enzyme states (E_2P) and $(E_2P)^*$. It has been shown before that this rate constant may be related to the radical pair recombination probability (for details and a comparison with experimental results see [21,46]):

$$k_{22,eff} = k_{22}(1 - P_R). \tag{3}$$

In this relation $(1 - P_R)$ represents the probability that the radical pair does not recombine. Consequently, the enzyme reaction cycle advances into the forward direction. The approach (Eq. (3)), enables the calculation of P_R by applying well-established models known from the theory of radical pair recombination. One possibility is to use the exponential model, which assumes that the radicals separate after a certain period of time and subsequent reencounters are neglected [23,24]. In the simplest case of a singlet–radical pair precursor with only one spin $1/2$ magnetic nucleus present and restriction to the high field limit ($B \gg A_{hfi}$ where B is magnetic flux density and A_{hfi} is the hyperfine interaction constant) this model yields [23]:

$$P_R(B) = \left(\frac{k_{-22}}{k_{-22} + k_{32}}\right) \bullet \left(\frac{1 + (C_1 + C_2)\Omega_s + C_1C_2\Omega_d^2}{1 + 2C_2\Omega_s + C_2^2\Omega_d^2}\right) \tag{4}$$

$$C_1 = \frac{1}{k_{32}} \frac{2k_{32} + k_{-22}}{(k_{32} + k_{-22}/2)^2 + (2J)^2},$$

$$C_2 = \frac{2k_{32} + k_{-22}}{k_{32} + k_{-22}} C_1,$$

where $\Omega_{s,d} = (\Delta\omega)^2 \pm (a/4)^2$. In this relation $2J$ corresponds to the energy splitting induced by the exchange interaction, a is the hyperfine interaction constant of the spin $1/2$ magnetic nucleus, and $\Delta\omega = (\mu_B/\hbar)B\ \Delta g/2$ refers to the Δg — mechanism (for review see [22–25]). In the case of oscillating magnetic fields varying at a frequency that is much smaller than the reciprocal of the radical pair lifetime, one may substitute the actual value of $B(t)$ to calculate the recombination probability and the effective rate constant $k_{22,\mathrm{eff}}$.

So far properties of the model were described that are related to the two enzyme reactions controlling the system. To complete the model a source term for substrate is included (see Fig. 1). This allows for the existence of a Hopf bifurcation and the occurrence of self-sustained oscillatory behavior [25]. Under steady state enzyme kinetics conditions with no magnetic field or static magnetic fields only present, the resulting differential equations read:

$$\frac{\mathrm{d}x}{\mathrm{d}t} = 1 - x - v_1(x) + v_2(y) \tag{5}$$

$$\frac{\mathrm{d}y}{\mathrm{d}t} = v_1(x) - v_2(y), \tag{6}$$

where $x = [S]/[S_0]$, $y = [P]/[S_0]$, and the following definitions are used:

$$v_1(x) = V_1 \frac{x}{\beta_1 + x(1 + \alpha x)},\ v_2(y) = V_2 \frac{y}{\beta_2 + y}, \tag{7}$$

$$V_1 = k_{21} \frac{[E_{1,\mathrm{total}}]}{\gamma[S_0]},\ V_2 = \frac{k_{22,\mathrm{eff}} k_{42}}{k_{22,\mathrm{eff}} + k_{42}} \frac{[E_{2,\mathrm{total}}]}{\gamma[S_0]}, \tag{8}$$

$$\beta_1 = \frac{k_{-11} + k_{21}}{k_{11}[S_0]},\ \beta_2 = \frac{k_{-12} + k_{22,\mathrm{eff}}}{k_{12}[S_0]} \frac{k_{42}}{k_{22,\mathrm{eff}} + k_{42}}, \tag{9}$$

$$\alpha = k_{-I}/k_I[S_0]. \tag{10}$$

In Eqs. (5) and (6) time is scaled in units of the rate constant γ.

The system exhibits a single steady state at $\{x_s, y_s\} = \{1, \beta_2 v_1(x_s)/(V_2 - v_1(x_s))\}$. The steady state loses its stability via a Hopf bifurcation at $1 + \partial v_1(x_s)/\partial x + \partial v_2(y_s)/\partial y = 0$.

In the case of magnetic fields varying on a time scale that is comparable to the one for processes within the enzyme reaction cycle — other than those connected with the spin evolution of the radical pair states — it becomes necessary to extend the model (Eq. (5) and (6)), and to explicitly integrate the time evolution of the enzyme intermediates. To simplify calculations in the following, we neglect reversible enzyme–substrate association processes ($k_{-11} = k_{-12} = 0$). Furthermore, we assume a rapid equilibrium for the intermediate states (SE_1S) corresponding to E_1 (see Eq. (1)) and $(E_2P)^*$ corresponding to E_2 (see Eq. (2)). These conditions are achieved if $k_{-I}/k_I \gg 1$ and $k_{42}/k_{22,\mathrm{eff}} \gg 1$. The assumptions simplify calculations without changing the basic results of the model simulations. Using the same definitions as before and defining further: $e_1 = [(E_1S)]/[E_{1,\mathrm{total}}]$, $e_2 = [(E_2P)]/[E_{2,\mathrm{total}}]$, $\mu_1 = k_{11}[E_{1,\mathrm{total}}]/\gamma$, $\mu_2 = k_{12}[E_{2,\mathrm{total}}]/\gamma$, $\eta_1 = k_{21}[E_{1,\mathrm{total}}]/\gamma[S_0]$, $\eta_2 = k_{22,\mathrm{eff}}[E_{2,\mathrm{total}}]/\gamma[S_0]$, $\epsilon_1 = [E_{1,\mathrm{total}}]/[S_0]$, $\epsilon_2 = [\mathrm{E}_{2,\mathrm{total}}]/[S_0]$, the following set of differential equations is obtained:

$$\frac{\mathrm{d}x}{\mathrm{d}t} = 1 - x - u_{11} + u_{22} \tag{11}$$

$$\frac{\mathrm{d}y}{\mathrm{d}t} = -u_{12} + u_{21} \tag{12}$$

$$\epsilon_1 \frac{\mathrm{d}e_1}{\mathrm{d}t} = u_{11} - u_{21} \tag{13}$$

$$\epsilon_2 \frac{\mathrm{d}e_2}{\mathrm{d}t} = u_{12} - u_{22}, \tag{14}$$

where:

$$u_{11} = \mu_1 x(1 - e_1(1 + \alpha x)),\ u_{12} = \mu_2 y(1 - e_2), \tag{15}$$

$$u_{21} = \eta_1 e_1,\ u_{22} = \eta_2 e_2. \tag{16}$$

The system consisting of Eqs. (11)–(16) forms the basis for the model simulations outlined in the following section. The model combines a detailed description of the primary physical interaction mechanism that couples the external magnetic field to the biological system. In this regard Eq. (4) is used to calculate the radical pair recombination probability in dependence on magnetic flux density. Eq. (4) refers to a well-established model based on quantum-statistical calculations for the radical pair states. This approach enables the calculation of an effective rate constant $k_{22,\mathrm{eff}}$ (Eq. (3)), that characterizes net forward flux within the enzyme reaction cycle. The secondary biological change is investigated with the equations describing the chemical kinetics of the system, Eqs. (11)–(16). The latter include a regulatory feedback mechanism and a source term for substrate. These conditions enable the occurrence of self-sustained oscillatory behavior. In this way one finally arrives at a model that combines both a microscopic description of physical interactions and macroscopic non-linear dynamics. The approach thus allows the study of external magnetic field perturbations on a non-linear dynamical biochemical reaction.

3. Results and discussion

3.1. Oscillatory biochemical reactions and magnetic field effects

The ratio of the Michaelis–Menten constants defined as $\epsilon = \beta_1/\beta_2$ (Eq. (9)) yields a measure of the time scales associated with the two enzyme reactions. The condition $\epsilon \ll 1$ leads to the typical relaxation-oscillator type of behavior. In this case the variable x corresponds to a fast 'switching variable', whereas y represents a slow 'reservoir variable'. The parameter γ scales the time in proportion to the input. Therefore the model system exhibits frequency encoding properties, meaning that the oscillation period is sensitive towards variations of γ [49].

The potential for frequency encoding has been found in a number of enzyme-regulated oscillatory systems. One example is again the cytosolic calcium oscillator, which is of the relaxation oscillator type [49]. This system exhibits frequency encoding properties, that is, in a number of cell types the oscillation period is a function of the strength of the external biochemical stimulus [50,51]. Significantly, it has been recently reported that the period of cytosolic calcium oscillations can indeed determine the degree of gene activation [6,7]. This finding lends strong support to the notion of a functional role for frequency-encoded signals at the level of the single cell. The peroxidase oscillator system is also a relaxation type system, but its biological function, if any, remains unknown. In this case only a single enzyme is involved. However, the reaction network of the oscillator includes two coupled feedback loops [9,52]. Therefore processes operating on different time scales are again distributed throughout the reaction network enabling the generation of complex oscillatory dynamics as in the case of the calcium oscillator. Other examples include glycolytic oscillations and oscillations of cyclic AMP (for recent overviews of such biochemical oscillators see [53,54]).

The parameter combination resulting in self-sustained oscillatory behavior may easily be obtained from the two-dimensional system (Eqs. (5)–(10)). The parameter values are chosen to yield an oscillation period of $T \approx 100$ s. By comparison with the two-dimensional system the parameter values of the four-dimensional model (Eqs. (11)–(16)) may be determined, too. However, here one also needs to specify the parameters describing the radical pair states (see Eq. (4)). To keep calculations simple, we restrict the following discussion to the Δg mechanism [22–25]. This mechanism leads to coherent spin mixing between the singlet and triplet T_0 states because of different g values of the radicals ($a = 0$ in Eq. (4)). In this example the radical pair recombination probability reads as follows:

$$P_R(B) = \left(\frac{k_{-22}}{k_{-22} + k_{32}}\right)\left(\frac{1 + C_1(\Delta\omega)^2}{1 + C_2(\Delta\omega)^2}\right), \qquad (17)$$

where magnetic flux density is given as $B(t) = B_{DC} + B_{AC}\cos(\omega_{AC}t)$. To characterize the radical pair states, parameter values are used that are

similar to experimentally obtained values for the {5′-deoxyadenosyl, cob(II)alamin}-radical pair produced by enzyme-induced homolysis of the C–Co bond of coenzyme B_{12}-dependent ethanolamine ammonia lyase (for details see [16,18,19,55]).

Fig. 2 depicts an oscillation diagram of the unperturbed system. The diagram reveals that there are long intermediate phases wherein the substrate concentration only moderately increases. At the same time the product concentration gradually increases. A threshold is reached after the inhibitory effect of substrate on E_1 becomes effective ($x > 1/\sqrt{2}$). In this phase product concentration is not increasing further thus resulting in an accumulation of substrate and in the formation of a spike. The subsequent removal of substrate terminates the spike and resets the cycle.

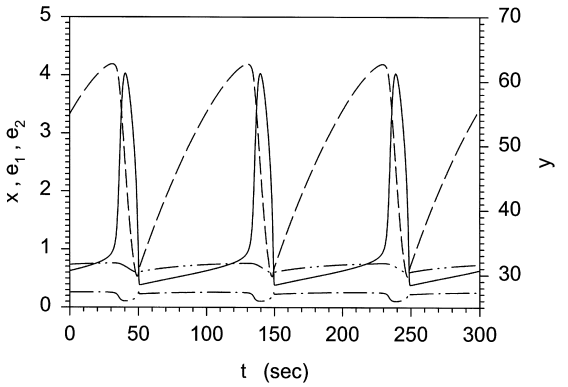

Fig. 2. Oscillation diagram of the substrate and product concentrations and of two intermediate enzyme–substrate complexes. The lines represent the temporal evolution of: substrate concentration (solid line, x); product concentration (dashed line, y); concentration of intermediate enzyme–substrate complex corresponding to enzyme E_1 (dash-dotted line, e_1); concentration of intermediate enzyme–substrate complex corresponding to enzyme E_2 (dash-dot-dotted line, e_2). Parameters: $\eta_1 = 24$, $\mu_1 = 24$, $\alpha = 2$, $\eta_2 = 8$, $\mu_2 = 0.4$, $\epsilon_1 = 0.1$, $\epsilon_2 = 0.1$, $k_{-22} = 10^9\ s^{-1}$, $k_{32} = 10^8\ s^{-1}$, $2J = 0$, $a = 0$, $\Delta g = 0.25$. The differential equations were integrated by applying different numerical methods and programs written in the Fortran and C programming languages. The integration was performed with an adaptive stepsize fifth-order Cash–Karp Runge–Kutta method, as well as with a semi-implicit extrapolation method developed by Bader and Deuflhard (for details see [56]). No difference in results were observed between the two methods.

In Fig. 3 the effect of static magnetic fields on the recombination probability of the radical pair and on the oscillation period is shown. One observes that a magnetic flux density of $B_{DC} = 10$ mT induces a reduction of the oscillation period of approx. 50%. At the same time the recombination probability is reduced by only 2.5%. This shows that the kinetic properties of the enzyme reactions provide a basis for amplifying small initial changes induced by the primary physical interaction mechanism. The reason for this behavior is that both kinetic parameters of enzyme E_2, that is, the maximum reaction velocity V_2 and the Michaelis–Menten constant β_2 depend on magnetic flux density via the rate constant $k_{22,\mathrm{eff}}$ (see Eqs. (8),(9)). Therefore small changes in the recombination probability, leading to equivalent changes in $k_{22,\mathrm{eff}}$ (see Eq. (4)), may result in much greater influences on the enzyme reaction and the resulting oscillation periods. Because the Δg mechanism leads to an increase in the triplet T_0 population, from which recombination into the (E_2P) state is not possible due to the Pauli principle, the net cycling of the system increases. This finally results in the observed decrease of the oscillation period. The effects are quite remarkable. To reduce the oscillation period by an equivalent amount of approx. 50% by variation of the chemical boundary conditions, one would have to increase the rate of substrate supply by approx. 40%. This change may be achieved by increasing the rate constant γ.

The results obtained with static magnetic fields reveal a specific sensitivity of the oscillator towards magnetic field influences. To further explore this aspect time-dependent magnetic fields may be applied. In this case one may expect direct influences on the non-linear dynamical behavior of the oscillator. In particular, a frequency-dependent response behavior to the external perturbation may be observed. Fig. 4 summarizes the simulation results. In Fig. 4a the magnetic flux density is fixed at $B_{AC} = 12$ mT and the field frequency is varied, whereas in Fig. 4b the field frequency is fixed at $\omega_{AC} = 0.25\ s^{-1}$ and magnetic flux density is increased. This value of the field frequency equals approximately four times the limit cycle frequency of the unper-

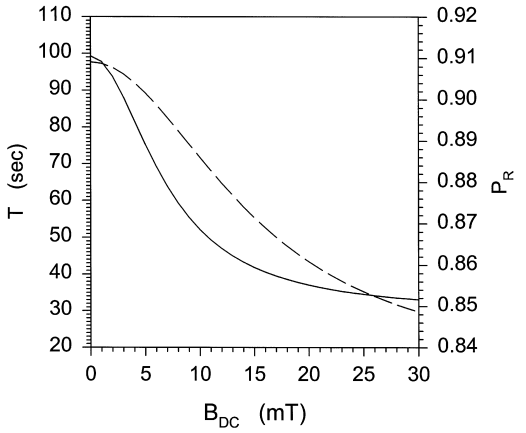

Fig. 3. Response behavior of the oscillator towards static magnetic field, $B = B_{DC}$, perturbations. The solid line refers to the oscillation period. The dashed line represents the radical pair recombination probability. Note the different axis-scaling. Parameters are the same as in Fig. 2.

turbed system. The latter is indicated by the arrow on the bottom diagram of Fig. 4a ($\omega_0 \approx 0.063$ s^{-1}). The top diagrams in Fig. 4 depict the oscillation amplitudes. Only amplitudes exceeding the threshold $x_{th} = 2.0$ are shown. The existence of a cut-off is based on the assumption that a detector that is capable of processing information from the oscillations only responds to spike inputs exceeding a certain threshold. The actual value of this cut off is arbitrarily chosen, because so far no detector structure has been specified. The bottom diagrams in Fig. 4 depict the oscillation periods of the resulting patterns, normalized to the external field period.

Fig. 4 reveals that in both cases the time-varying magnetic field perturbation induces a complex sequence of alternating periodic (resonant) and non-periodic (quasiperiodic and chaotic) oscillation patterns. Some representative oscillation patterns are shown in Fig. 5. In principle, the resulting behavior yields a number of standard features known from externally driven self-sustained oscillators. However, it has to be taken into account that in the present case the external driver is not just an additive term in the model equations. Rather the coupling of the magnetic field leads to a parametrically-driven system. Furthermore, Eq. (16) reveals that the recombination probability, and consequently the parameter η_2 in the model (Eqs. (10)–(15)), exhibit a quadratic dependence on the magnetic flux density. As a result the enzyme reaction E_2 actually senses a frequency-doubled perturbation. This may also be recognized in the properties of the resulting oscillation patterns. The oscillator displays periodic states predominantly at frequency intervals wherein the ratio between the internal oscillation period and the one of the external field equals $N/2$, ($N = 1,2,3,...$; see bottom diagrams in Fig. 4). Specifically at field frequencies close to the unperturbed limit cycle frequency a resonant state with $T/T_{AC} = 1/2$ exists.

Comparable to the static magnetic field case, the changes induced on the radical recombination probability are rather small. Indeed, the temporal variations of the recombination probability obtained with the parameter values applied in Fig. 4a are in the order of 3.2% (difference min/max amplitude). Again these small variations induced by the primary physical interaction mechanism may lead to profound changes in the secondary (biologically relevant) response behavior of the system.

The response patterns reveal several other interesting features. In the case where the magnetic flux density is fixed and the field frequency varies one observes a frequency-dependent response behavior. Within the periodic states the response amplitudes display a maximal value at the low-frequency end of the resonance intervals. The amplitudes gradually decrease towards the high-frequency end of the intervals. This behavior continues until, close to a field frequency that is 10 times higher than the unperturbed limit cycle frequency, there is a sudden transition into a state exhibiting oscillation amplitudes below the threshold defined above (Fig. 5e). In this state the individual features of the unperturbed oscillator are lost. The system is forced into a sinusoidal oscillation that follows the external field variations around the steady state value at $x_s = 1$. This behavior is quite remarkable, because it occurs at a relatively high external field frequency in comparison to the unperturbed limit cycle frequency. Model simulations reveal that such an oscillation pattern may still be observed even if the internal

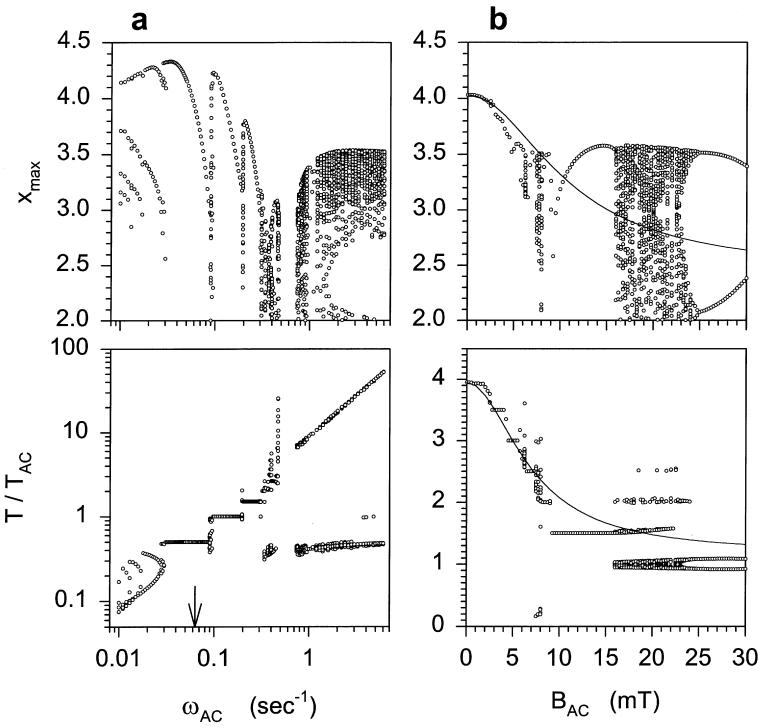

Fig. 4. Response behavior of the oscillator towards oscillating magnetic field, $B(t) = B_{AC}\cos(\omega_{AC}t)$, perturbations. a: *top* Response amplitudes; *bottom* oscillation periods as a function of the applied field frequency at a fixed magnetic flux density. The arrow in the bottom diagram represents the limit-cycle frequency of the unperturbed oscillator. b: *top* Response amplitudes; *bottom* oscillation periods as a function of the applied magnetic flux density at a fixed field frequency. The lines correspond to the response behavior towards static magnetic field perturbations (compare Fig. 3). Parameters are the same as in Fig. 2, except: (a) $B_{AC} = 12$ mT, (b) $\omega_{AC} = 0.25$ s^{-1}. The differential equations were integrated applying the techniques described in the caption to Fig. 2. Different integration stepsizes were applied to check the accuracy of the results. No major differences or co-existing solutions were observed.

period of the system is much longer than the one obtained with the parameter combination applied so far. For example, setting $\beta_2 = 0.01$ yields a limit cycle period of $T \approx 2870$ s. Applying the same combination of field parameters to the system still induces a transition into an oscillation pattern that is similar to the one shown in Fig. 5e. The transition into the sinusoidal oscillation around the steady state is performed via an intermittent type of behavior. Fig. 5d shows the resulting oscillation pattern at a frequency slightly below the transition. In this case the oscillation pattern displays long laminar phases that are interrupted by large-amplitude bursts.

Increasing the field frequency beyond the region discussed above leads to the formation of a pattern that is a superposition of large amplitude spikes and small oscillations (Fig. 5f). The latter exhibit twice the frequency of the external field, because of the quadratic dependence of the recombination probability on magnetic flux density. The interval between the large amplitude spikes corresponds to one that may be obtained by substituting $B_{DC} = B_{AC}/\sqrt{2}$. The factor $\sqrt{2}$ results from replacing the squared cosine function by its time-average. This shows that at frequencies that are much greater than the internal limit-cycle frequency the time-varying magnetic field effect is to a large extent equivalent to the corresponding effect of a static magnetic field of lower amplitude.

In the case where the field frequency is fixed and the magnetic flux density increases, the oscillator also displays a number of periodic states

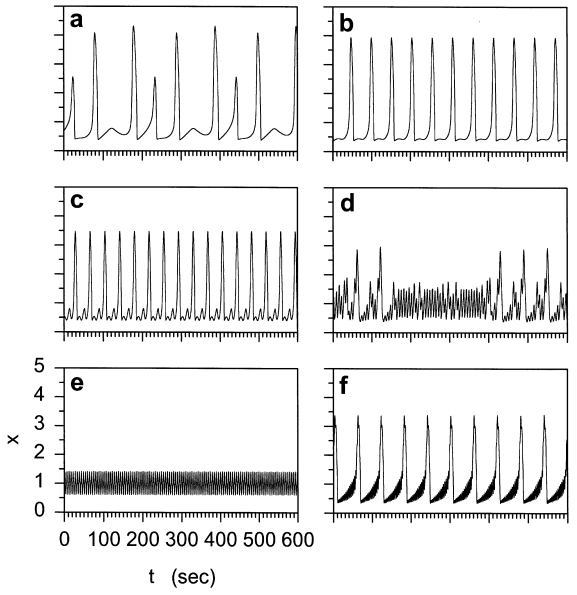

Fig. 5. Oscillation diagrams in response towards oscillating magnetic field, $B(t) = B_{AC}\cos(\omega_{AC}t)$, perturbations. Parameters are the same as in Fig. 4a, except: (a) $\omega_{AC} = 0.03\ s^{-1}$; (b) $\omega_{AC} = 0.06\ s^{-1}$; (c) $\omega_{AC} = 0.25\ s^{-1}$; (d) $\omega_{AC} = 0.47\ s^{-1}$; (e) $\omega_{AC} = 0.6\ s^{-1}$; (f) $\omega_{AC} = 1.0\ s^{-1}$.

wherein the ratio between the internal oscillation period and the one of the external field equals $N/2$ (Fig. 4b, $N = 1,2,3,...,7$). Specifically the interval with $T/T_{AC} = 3/2$ extends over a wide range of magnetic flux densities, ranging between $9\ \text{mT} < B_{AC} < 16\ \text{mT}$. If only, however, the biologically relevant information is contained within the interspike intervals, then within this interval an increase of the magnetic flux density would not produce a different effect on the biological system. Finally, at higher magnetic flux densities above $B_{AC} = 24$ mT the oscillator settles into a period-doubled state with $T/T_{AC} = 2/2$.

So far we discussed the response behavior of the oscillator to external magnetic field perturbations from the perspective of non-linear dynamics. Depending on the specific combination of static and/or time-varying field amplitudes and field frequency different oscillation patterns may be observed. In all cases the substrate concentration remains the same on temporal average, that is, $\langle x\rangle_t = x_s = 1$. This is because of the coupling of the system to the environment via the term $\gamma(S_0 - S)$, leading to a buffering effect of substrate concentration.

Despite the fact that the average substrate concentration remains constant, the cycling within the system is different, because of the parametrical coupling of the magnetic field and the inherent non-linearities. This means that depending on the field frequency the efficiency and the dissipation within the system are altered. Consequently, the average product concentration and the average product formation rate given by $\langle u_{21}(t)\rangle_t = \eta_1\langle e_1\rangle_t$ are altered, too. The characterization of the response behavior of externally driven systems by means of the dissipation or efficiency of the system has been utilized in a number of investigations before. Examples include theoretical studies of externally driven non-linear oscillators [57–60] as well as experimental studies of the externally perturbed peroxidase–oxidase reaction [3,8,37,38,40].

To investigate the response behavior of the system by the dissipation, we refer to the model given by Eqs. (5)–(10). The rates of substrate to product interconversion are given as v_1 and v_2, respectively (Eq. (7)). The dissipation of this process may be defined as follows (for details see [57,59]):

$$D_{SP} = (v_1 - v_2)RT\ \ln\left(\frac{v_1}{v_2}\right). \tag{18}$$

where T is temperature. Fig. 6 depicts the change of the dissipation in comparison to the unperturbed oscillator value in dependence on field frequency. Again one observes a frequency-dependent response behavior. In particular, within the resonant states the dissipation is increased in the middle of the resonance intervals and decreased towards the ends near the bifurcation into new states. The complex oscillatory states including those that separate the resonant ones are characterized by a decreased dissipation. Interestingly, the state where the system is forced into the sinusoidal oscillation around the steady state near $\omega_{AC} = 0.6\ s^{-1}$ results in a drastically decreased dissipation. This factor may contribute to the specific stability of this state.

Any change in the dissipation of the system is

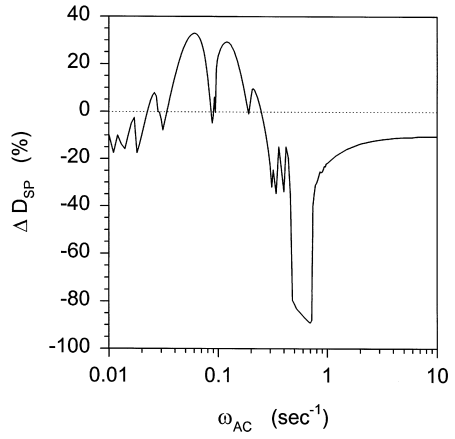

Fig. 6. Change in the dissipation of the system in response towards oscillating magnetic field, $B(t) = {}_{AC}\cos(\omega_{AC} t)$, perturbations. The dissipation is defined by Eq. (18). The example corresponds to the simulation results depicted in Fig. 4a. Parameters are the same as in Fig. 4a.

accompanied by changes in the average product concentration and in the average product formation rate. Thus the results shown in Fig. 6 demonstrate that the external perturbation induced by the oscillating magnetic field may effectively alter the efficiency of the system. Similar conclusions have been reached in the experimental studies of the peroxidase–oxidase system [3,37]. However, in these studies perturbations in the oxygen supply to the reaction of relatively high amplitudes had to be applied to achieve significant changes in the average dissipation. In the present model the external perturbation leads to a parametrical coupling. It appears that the parametric coupling of the oscillating magnetic field enables a very efficient form of perturbation of the system, in particular, considering the fact that the absolute modulation of the radical pair recombination probability is rather small.

3.2. Model of a biochemical decoding mechanism for oscillatory input

In the previous section the response behavior of the oscillator towards static and time-varying magnetic field perturbations is discussed. The results show that the system exhibits great sensitivity. In particular, a variety of characteristic response patterns are observed in response to time-varying magnetic fields. The question arises under which conditions of different oscillation patterns may produce different and biologically relevant changes. To establish such a connection a biological detection mechanism has to exist that is capable of responding to changes in the output of the oscillator. In this context the term output may refer to temporal variations of the substrate concentration as well as to those of the product concentration. In the following the situation where the temporal variations of substrate concentration represent the output is investigated. Specifically a decoding mechanism consisting of a protein system that acts as a molecular switch in response to substrate variations is studied. The model is shown in the following scheme:

$$\text{activation}: M_i \overset{k_a s^n}{\rightarrow} M_a,\ \text{deactivation}: M_a \overset{k_d}{\rightarrow} M_i, \tag{19}$$

where $[M_{\text{total}}] = [M_i] + [M_a] = \text{constant}$. The exponent n represents the degree of cooperativity in the activation process. In the model simulations a value of $n = 4$ is assumed. This corresponds to the properties of calmodulin, which has four bindings sites for calcium [61]. This example is closely related to the decoding of calcium signals. In this case calcium-dependent proteins such as calmodulin may operate as coupling elements. Enzyme systems that are regulated by the activity of calmodulin may further process the oscillatory input. For example, as one possible candidate calcium/calmodulin-dependent protein kinase II (CaM kinase II) has been considered to function as a frequency decoder for calcium oscillations [62–64]. Recent in-vitro experiments have confirmed that CaM kinase II activity is highly sensitive towards periodic oscillations in calcium concentration in the frequency range $\nu = 0.5$–4 Hz [65]. This finding may be related to the results mentioned before, where the oscillatory calcium input was processed as a frequency-encoding signal that induced or enhanced calcium-dependent gene activation events depending on the frequency of oscillations in cytosolic calcium concentration [6].

Defining $z = [M_a]/[M_{\text{total}}]$, $\kappa_a = k_a/\gamma$, $\kappa_d = k_d/\gamma$, one obtains the following differential equation for the detector:

$$\frac{dz}{dt} = \kappa_a [S_0]^n (1-z) x^n - \kappa_d z, \qquad (20)$$

where $x = [S]/[S_0]$, as before. Eq. (20) is added to the previous model defined by Eqs. (11)–(16). It is assumed that the total concentration of detector proteins is small compared to the substrate concentration. In this case one may neglect the proportion of substrate bound to the detector protein, and no further contribution has to be added to the differential equations describing substrate dynamics.

There are two principal ways the detector may function. The system may operate as an integrator that adds up successive input spikes. This leads to a slow increase in the fraction of activated proteins. In this case the detector is responsive to the amplitude of the input rather than to its frequency. In the second mode of operation the detector effectively switches between states of low activity ($z \to 0$) and high activity ($z \to 1$). In Fig. 7 the two cases are illustrated. The figure reveals that because of the cooperativity in the activation process there is a sharp increase in the fraction of activated proteins within the rising phase of the input spike. However, fluctuations not exceeding a certain threshold do not produce a response of the detector. The simulations displayed in Fig. 7 reveal that a value of $x_{\text{th}} \approx 2$ may be assigned as activation threshold. This value corresponds to the one that is applied in the simulations shown in Fig. 4.

In both modes of detector operation discussed in Fig. 7 the ratio between the activation rate constant, κ_a $[S_0^n]$, and the deactivation rate constant, κ_d, is the same. This means that in both examples the Michaelis–Menten constant and consequently the steady state concentration of activated proteins are the same. However, because the input signal is a time-dependent dynamical one, the detector does attain its steady state value. This behavior is illustrated in Fig. 8. The figure reveals that the mean concentration of activated proteins may be much greater than the

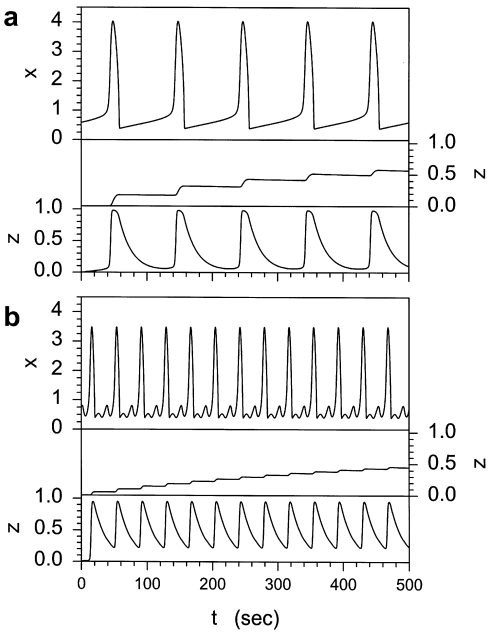

Fig. 7. Response behavior of the protein detector. The model of an activation/deactivation cycle of a protein is described by the reaction scheme given in Eq. (19). The figure depicts the oscillatory input (variable x, top diagrams in (a) and (b)) and the response of the protein detector. In the middle diagrams in (a) and (b) the detector kinetics are slow, whereas in the bottom diagrams they are fast. a: Response behavior without external perturbations. b: Response behavior in the presence of an oscillating magnetic field. Parameters are the same as in Fig. 2, furthermore: (b) $B_{AC} = 12$ mT, $\omega_{AC} = 0.25\ \text{s}^{-1}$; middle diagrams in (a) and (b): $\kappa_a\ S_0^n = 0.0001$, $\kappa_d = 0.0005$; bottom diagrams in (a) and (b): $\kappa_a S_0^n = 0.01$, $\kappa_d = 0.05$.

steady state value at $z_s = 1/6$. The latter is only reached if the detector kinetics are very fast, that is, if the switching between low- and high-activity states occurs on a time scale that is comparable to the variations of the input signal. These results show that the kinetic features of the detector critically determine its response behavior.

Based on these findings it is conceivable that the presence of the magnetic field may induce further changes, depending on the detector properties. Results shown in Fig. 8 reveal that for both static, as well as oscillating magnetic field perturbations, a biphasic change in the mean concentration of activated detector proteins results. This means that a decrease may be observed if kinetics are slow and the detector operates as

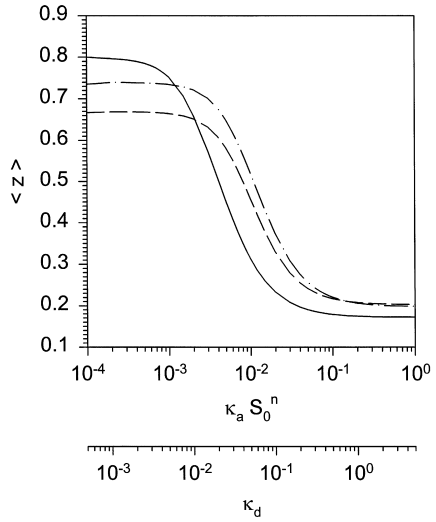

Fig. 8. Average concentration of activated receptor proteins as a function of the kinetic parameters of the system. The solid line depicts the case without external perturbations. The dashed line represents the response in the presence of a static magnetic field, $B = B_{DC}$, whereas the dash-dotted line represents the response in the presence of an oscillating magnetic field, $B(t) = B_{AC}\ \cos\ (\omega_{AC} t)$, perturbation. Note that the Michaelis–Menten constant, that is, the ratio $\kappa_a S_0^n/\kappa_d$ remains constant. Parameters are the same as in Fig. 2, except: $B_{DC} = 12$ mT, $B_{AC} = 12$ mT, $\omega_{AC} = 0.25\ s^{-1}$.

an integrator. For the parameter combination applied in the simulations shown in Fig. 8, a maximal decrease of approx. 17% results in the static magnetic field case, whereas with oscillating magnetic fields a maximal decrease of only 8% may be observed. The reason for the decrease is that the oscillation amplitudes are smaller in the presence of the field. These changes are greater in the static magnetic field case for the parameter values applied. In the opposite situation, that is, if the kinetics are fast the mean concentration of activated detector proteins is increased in the presence of the field. In this case a maximal increase of approx. 47% may be found with static magnetic fields, whereas with oscillating magnetic fields the increase is even more profound, that is, on the order of 67%.

4. Summary and outlook

The results discussed in the preceding sections show that the overall response behavior towards magnetic field perturbations of the combined system, consisting of the two coupled enzyme reactions and the detector protein, is critically determined by: (1) the specific combination of external field parameters (static and oscillating magnetic field amplitudes, field frequency); and (2) the kinetic properties of every subsystem. Simulations suggest that moderate-strength magnetic fields ($B = 1$–100 mT) may suffice to achieve significant changes in the response behavior of the system. Several levels of complexity have to be considered. First, at the stage of the initial coupling of the external magnetic field, the time scales associated with the spin evolution of the radical pair determine the size of the primary magnetic field effect. These initial changes are transduced into the system via modifications in the net forward flux of the magnetic field-sensitive enzyme. The kinetic features of the two coupled enzyme reactions determine the resulting influence on the oscillatory reaction. In particular, application of static magnetic fields may drastically change the oscillator period. Oscillating magnetic field perturbations may induce complex response patterns, depending on the field amplitude and frequency. Because of the differences in time scales associated with the two enzyme-regulated processes, field frequencies that are much greater than the autonomous limit-cycle frequency (for example by a factor of 10^2) may still be effective in controlling the oscillator. Finally, the kinetic properties of the detector mechanism critically determine the changes that may be observable on a macroscopic scale. In summary, the different parts of the model involve processes spanning a range of time scales that are separated by a factor of 10^{11}. Specifically, the time scales range from the nanosecond time domain (spin kinetics) to sub-second processes approx. 10^{-5} s to 1 s (enzyme kinetics), and finally processes on the order of minutes (oscillator period).

As outlined in Section 1, the peroxidase–oxidase oscillator has been utilized as a model system in experimental studies of the response behavior of biochemical oscillators towards time varying external perturbations. However, so far only chemical stimuli and in one study electric

currents have been applied to perturb the system. The recent discovery of the sensitivity of the redox cycle of horseradish peroxidase towards moderate-strength magnetic field exposures has opened up the opportunity of extending the above-mentioned studies to include oscillating magnetic fields as a novel type of perturbation. For this reason we have recently initiated a program with the goal of experimentally investigating the potential use of magnetic field perturbations as a tool for studying oscillatory enzyme dynamics based on the peroxidase–oxidase oscillator. These experimental studies may be supplemented by theoretical investigations that extend existing models of the peroxidase–oxidase oscillator by including microscopic interactions accounting for the primary magnetic field coupling to the system (Eichwald and Walleczek, unpublished results). The approach outlined in this paper may also serve as a guideline for these developments.

Acknowledgements

C.E. was a recipient of a Fetzer Institute Postdoctoral Fellowship. Work at the Bioelectromagnetics Laboratory is supported by the Fetzer Institute and the US Department of Energy.

References

[1] V. Petrov, V. Gáspár, J. Masere, K. Showalter, Nature (London) 361 (1993) 240.
[2] O. Steinbock, V. Zykov, S.C. Müller, Nature (London) 366 (1993) 322.
[3] J.G. Lazar, J. Ross, Science 247 (1990) 189.
[4] A. Garfinkel, L.M. Spano, W.L. Ditto, J.N. Weiss, Science 257 (1992) 1230.
[5] S.J. Schiff, K. Jerger, D.H. Duong, T. Chang, M.L. Spano, W.L. Ditto, Nature (London) 370 (1994) 615.
[6] R.E. Dolmetsch, K. Xu, R.S. Lewis, Nature (London) 392 (1998) 933.
[7] W. Li, J. Llopis, M. Whitney, G. Zlokarnik, R.Y. Tsien, Nature (London) 392 (1998) 936.
[8] A. Förster, T. Hauck, F.W. Schneider, J. Phys. Chem. 98 (1994) 184.
[9] R. Larter, L.F. Olsen, C.G. Steinmetz, T. Geest, in: R. Field, L. Györgyi (Eds.), Chaos in Chemistry and Biology, World Scientific, London, 1993 p. 175.
[10] H. Tributsch, R.A. Bogomolni, Chem. Phys. Lett. 227 (1994) 74.
[11] O. Steinbock, J. Schütze, S.C. Müller, Phys. Rev. Lett. 68 (1992) 248.
[12] V. Petrov, Q. Ouyang, H.L. Swinney, Nature (London) 388 (1997) 655.
[13] J. Hescheler, R. Speicher, Eur. Biophys. J. 17 (1989) 273.
[14] J. Haag, A. Borst, Nature (London) 379 (1996) 639.
[15] A. Förster, K.-P. Zeyer, F.W. Schneider, J. Phys. Chem. 99 (1995) 11889.
[16] C.B. Grissom, Chem. Rev. 95 (1995) 3.
[17] J. Walleczek, in: M. Blank (Ed.), Advances in Chemistry No. 250 — Electromagnetic Fields: Biological Interactions and Mechanisms, American Chemical Society, Washington DC, 1995, p. 395.
[18] T.T. Harkins, C.B. Grissom, Science 263 (1994) 958.
[19] T.T. Harkins, C.B. Grissom, J. Am. Chem. Soc. 117 (1995) 566.
[20] M.B. Taraban, T.V. Leshina, M.A. Anderson, C.B. Grissom, J. Am. Chem. Soc. 119 (1997) 5768.
[21] C. Eichwald, J. Walleczek, Biophys. J. 71 (1996) 623.
[22] N.J. Turro, Proc. Natl. Acad. Sci. U.S.A. 80 (1983) 609.
[23] K.M. Salikhov, Y.N. Molin, R.Z. Sagdeev, A.L. Buchachenko, Spin Polarization and Magnetic Field Effects in Radical Reactions, Elsevier, Amsterdam, 1984.
[24] U.E. Steiner, T. Ulrich, Chem. Rev. 89 (1989) 51.
[25] K.A. McLauchlan, U.E. Steiner, Mol. Phys. 73 (1991) 241.
[26] R.D. Astumian, M. Bier, Biophys. J. 70 (1996) 637.
[27] A. Arkin, J. Ross, Biophys. J. 67 (1994) 560.
[28] D. Bray, Nature (London) 376 (1995) 307.
[29] E.R. Stadtman, P.B. Chock, Proc. Natl. Acad. Sci. U.S.A. 74 (1977) 2761.
[30] E. Shacter, P.B. Chock, E.R. Stadtman, J. Biol. Chem. 259 (1984) 12252.
[31] A. Goldbeter, D.E. Koshland, Jr., Proc. Natl. Acad. Sci. U.S.A. 78 (1981) 6840.
[32] A. Goldbeter, D.E. Koshland, Jr., J. Biol. Chem. 259 (1984) 14441.
[33] M. Okamoto, T. Sakai, K. Hayashi, Biol. Cybern. 58 (1988) 295.
[34] A. Hjelmfelt, E.D. Weinberger, J. Ross, Proc. Natl. Acad. Sci. U.S.A. 88 (1991) 10983.
[35] M.J. Berridge, Nature (London) 361 (1993) 315.
[36] D.E. Clapham, Cell 80 (1995) 259.
[37] J.G. Lazar, J. Ross, J. Chem. Phys. 92 (1990) 3579.
[38] M.S. Samples, Y.-F. Hung, J. Ross, J. Phys. Chem. 96 (1992) 7338.
[39] T. Hauck, F.W. Schneider, J. Phys. Chem. 97 (1993) 391.
[40] T. Hauck, F.W. Schneider, J. Phys. Chem. 98 (1994) 2072.
[41] A. Lekebusch, A. Förster, F.W. Schneider, J. Phys. Chem. 99 (1995) 681.
[42] A. Förster, M. Merget, F.W. Schneider, J. Phys. Chem. 100 (1996) 4442.
[43] P. Shen, R. Larter, Biophys. J. 67 (1994) 1414.
[44] J. Keizer, Biophys. J. 65 (1993) 1359.
[45] H. Degn, Nature (London) 217 (1968) 1047.

[46] C. Eichwald, J. Walleczek, J. Chem. Phys. 107 (1997) 4943.
[47] C. Eichwald, J. Walleczek, Bioelectromagnetics 17 (1996) 427.
[48] B. Brocklehurst, K.A. McLauchlan, Int. J. Radiat. Biol. 69 (1996) 3.
[49] Y. Tang, H.G. Othmer, Proc. Natl. Acad. Sci. U.S.A. 92 (1995) 7869.
[50] M.J. Berridge, A. Galione, FASEB. J. 2 (1988) 3074.
[51] C. Schöfl, G. Brabant, R.-D. Hesch, A. von zur Mühlen, P.H. Cobbold, K.S.R. Cuthbertson, Am. J. Physiol. 265 (1993) C1030.
[52] D.L. Olson, E.P. Williksen, A. Scheeline, J. Am. Chem. Soc. 117 (1995) 2.
[53] I. Schreiber, Y.F. Hung, J. Ross, J. Phys. Chem. 100 (1990) 8556.
[54] A. Goldbeter, Biochemical Oscillations and Cellular Rhythms, Cambridge University Press, Cambridge, 1996.
[55] E. Natarajan, C.B. Grissom, Photochem. Photobiol. 64 (1996) 286.
[56] W.H. Press, S.A. Teukolsky, W.T. Vetterling, B.P. Flannery, Numerical Recipes in Fortran/Numerical Recipes in C, Cambridge University Press, Cambridge, 1992.
[57] Y. Termonia, J. Ross, Proc. Natl. Acad. Sci. U.S.A. 78 (1981) 2952.
[58] P.H. Richter, P. Rehmus, J. Ross, Prog. Theor. Phys. 66 (1981) 385.
[59] M. Schell, K. Kundu, J. Ross, Proc. Natl. Acad. Sci. U.S.A. 84 (1987) 424.
[60] F. Kaiser, in: H. Fröhlich (Ed.), Biological Coherence and Response to External Stimuli, Springer, Berlin, 1988, p. 224.
[61] L. Stryer, Biochemistry, W.H. Freeman and Company, New York, 1988.
[62] P.I. Hanson, T. Meyer, L. Stryer, H. Schulman, Neuron 12 (1994) 943.
[63] T. Matsushita, S. Moriyama, T. Fukai, Biol. Cybern. 72 (1995) 497.
[64] A. Dosemeci, R.W. Albers, Biophys. J. 70 (1996) 2493.
[65] P. De Koninck, H. Schulman, Science 279 (1998) 227.